

Summing Real Time Feynman Paths of Lattice Polaron with Matrix Product States

Qi Gao^{1,2} and Yuan Wan^{1,3,*}

¹*Institute of Physics, Chinese Academy of Sciences, Beijing 100190, China*

²*University of Chinese Academy of Sciences, Beijing 100049, China*

³*Songshan Lake Materials Laboratory, Dongguan, Guangdong 523808, China*

(Dated: July 11, 2025)

We study numerically the real time dynamics of lattice polarons by combining the Feynman path integral and the matrix product state (MPS) approach. By constructing and solving a flow equation, we show that the integrand, viewed as a multivariable function of polaron world line parameters, can be compressed as a low bond dimension MPS, thereby allowing for efficient evaluation of various dynamical observables. We establish the effectiveness of our method by benchmarking the calculated polaron spectral function in one dimension against available results. We further demonstrate its potential by presenting the polaron spectral function in two dimensions and simulating polaron diffusion in both one and two dimensions.

Introduction — Efficient simulation of quantum many-body dynamics is a long-standing problem in condensed matter physics [1–4]. The difficulties with this task are amply illustrated by a prototypical $N + 1$ body system, a polaron, which consists of an electron interacting with phonons. Instrumental in the historical development of many-body physics [5–8], it has received renewed attention [9–14] owing to its rich dynamical properties [15, 16] and potential connection to high-temperature superconductors [17–22] and solar cells [23–26].

Despite decades of progress [27], simulating the real time dynamics of polaron still faces obstacles. On one hand, Monte Carlo simulation in real time often encounters dynamical signs [28, 29]. While the sign-free imaginary time Monte Carlo is efficient and accurate in determining low energy properties of polaron [30, 31], accessing its spectral functions requires analytic continuation [32–35]. On the other hand, variational approaches using various wave function ansätze [36–42] including the matrix product state (MPS) [43–45] are successful in one dimension. Yet, going to higher spatial dimensions remains challenging [46–49]. In particular, the infinite local Hilbert space dimension of phonons needs proper truncation [38, 44].

In this work, we tackle the polaron dynamics problem by taking advantage of both path integral and MPS approaches. Focusing on the lattice polaron, we show that its real time Feynman path integral can be efficiently evaluated by casting it in MPS form (Fig. 1). A path integral is essentially a high dimensional sum $Q = \sum_{\{s\}} A(s_M, \dots, s_2, s_1)$, where the labels $\{s\}$ parametrize the world line and A is its quantum amplitude. By using a flow equation, we compress A as a low bond dimension MPS, $A(s_M, \dots, s_2, s_1) \approx A_M(s_M) \cdots A_2(s_2) A_1(s_1)$, and then sum it efficiently, $Q \approx \sum_{s_M} A_M(s_M) \cdots \sum_{s_2} A_2(s_2) \sum_{s_1} A_1(s_1)$. This method shares similar spirit with the tensor train method for high dimensional integration [50–54], as well as the tensor network influence functional approach to spatially local open quantum systems [55–57] and one-dimensional

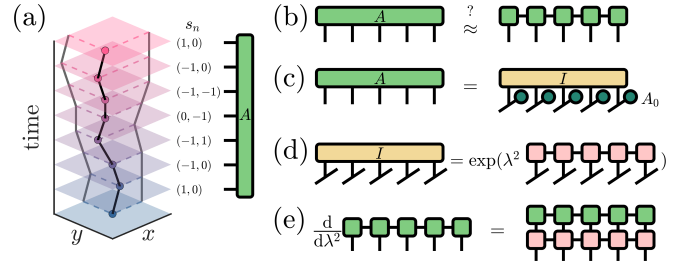


FIG. 1. MPS summation of real time Feynman paths. (a) World line of a polaron is parametrized by its displacements $\{s\}$ between successive times. Quantum amplitude A as a function of $\{s\}$ may be viewed as a high dimensional tensor. (b) A can be efficiently summed provided that it is well approximated by a low bond dimension MPS. (c) A is given by the free amplitude A_0 dressed by phonon influence functional I , which, in turn, is the exponential of a low bond dimension matrix product operator (d). (e) A satisfies an ordinary differential equation with respect to electron-phonon coupling λ^2 . Integrating it from $\lambda^2 = 0$ yields the MPS approximation to A .

systems [58–61], but features perspective and formulation that are unique to polarons.

Our method is sign tolerant, applicable to higher spatial dimensions, free from truncation in phonon Hilbert space, and admits various generalizations. We establish its effectiveness by benchmarking the polaron spectral function, calculated through real time evolution, against available results in one dimension. We further demonstrate its potential by computing the spectral function in two dimensions and taking a first pass at simulating a nonequilibrium diffusion process.

Setup — We use a one-dimensional polaron model to illustrate our method [62]; generalizations to higher dimensions will be straightforward. The Hamiltonian is $H = K + V$. K describes electron hopping in a chain of N sites subject to periodic boundary condition:

$$K = - \sum_i (c_i^\dagger c_{i+1} + c_{i+1}^\dagger c_i). \quad (1a)$$

c_i (c_i^\dagger) annihilates (creates) a spinless electron on site i . The hopping amplitude is set to 1. V describes the phonons and their coupling to electrons:

$$V = \sum_q [\omega_q b_q^\dagger b_q - \lambda f_q n_q (b_q + b_{-q}^\dagger)]. \quad (1b)$$

b_q (b_q^\dagger) annihilates (creates) a phonon with wave vector q . ω_q is the dispersion relation. The coupling constant $\lambda > 0$. The form factor $f_q = f_{-q}^*$. $n_q = \frac{1}{\sqrt{N}} \sum_k c_{k+q}^\dagger c_k$ is the Fourier transform of electron density operator. H conserves the total number of electrons $N_e = \sum_i c_i^\dagger c_i$.

The quantity of interest is the electron propagator :

$$iG^R(k, t) = \theta(t) \langle 0 | c_k e^{-iHt} c_k^\dagger | 0 \rangle. \quad (2)$$

$|0\rangle$ refers to the ground state of Eq. (1) in $N_e = 0$ sector. k is the electron wave vector. The Heaviside function $\theta(t)$ enforces the causality $t > 0$.

Path integral — We express $G^R(k, t)$ as a path integral. Trotterizing the time evolution to second order, and inserting partial resolution of identity by electron position eigenstates, we find [63]:

$$iG^R(k, t) = \theta(t) \sum_{\{x\}} e^{ikx_M} I(\{x\}) A_0(\{x\}). \quad (3a)$$

M is the number of time slices. $\{x\} = \{x_M, \dots, x_1, x_0\}$ are electron position at successive times. We impose the boundary condition $x_0 = 0$, whereas $x_{n \geq 1}$ is unrestricted. A_0 is the quantum amplitude for a free electron, $A_0(\{x\}) = \prod_{n=1}^M f(x_n - x_{n-1})$, with $f(x_n - x_{n-1}) = \langle x_n | e^{-i\epsilon K} | x_{n-1} \rangle$. $\epsilon = t/M$ is the Trotter time.

I is the phonon influence functional:

$$I(\{x\}) = \langle \phi | e^{-i\frac{\epsilon}{2}V(x_M)} \dots e^{-i\epsilon V(x_1)} e^{-i\frac{\epsilon}{2}V(x_0)} | \phi \rangle. \quad (3b)$$

$|\phi\rangle$ is the phonon vacuum. Here, we have used the fact that V commutes with electron coordinate x . $V(x)$ is the phonon Hamiltonian when the electron is located at x , $V(x) = \sum_q [\omega_q b_q^\dagger b_q - \frac{\lambda}{\sqrt{N}} (f_q e^{iqx} b_q + h.c.)]$.

We perform a change of variable from position to displacement $s_n = x_n - x_{n-1}$:

$$iG^R(k, t) = \theta(t) \sum_{\{s\}} \left(\prod_{n=1}^M e^{iks_n} \right) I(\{s\}) A_0(\{s\}). \quad (4a)$$

$\{s\} = \{s_M, \dots, s_2, s_1\}$. $A_0(\{s\}) = \prod_{n=1}^M f(s_n)$. Since $|f(s)| \sim O(\epsilon^{|s|})$, we restrict the summation over s_n to the range $|s_n| \leq 2$. The introduced error is on the same order as the Trotter error. As $\{s\}$ constitute the physical legs for the MPS, this truncation reduces the computational cost by decreasing the physical dimension.

We rewrite the phonon influence functional I in terms of $\{s\}$. We define a translation operator $T(a)$ that maps the phonon mode on site x to $x+a$. As a result, $V(x) = T(x)V(0)T(-x)$. Inserting it into Eq. (3b) yields,

$$I(\{s\}) = \langle \phi | U(s_M) \dots U(s_2) U(s_1) | \phi \rangle. \quad (4b)$$

$U(s) = e^{-i\frac{\epsilon}{2}V(0)} T(-s) e^{-i\frac{\epsilon}{2}V(0)}$ is an s -dependent unitary operator. This trick is amount to a change of reference frame from the phonons to the electron, and reminiscent of the Lee-Low-Pines transformation [64].

Eq. (4) is our starting point. We wish to compress the quantum amplitude $A(\{s\}) \equiv I(\{s\}) A_0(\{s\})$ as an MPS, $A(\{s\}) \approx A_M(s_M) \dots A_1(s_1)$ (Fig. 1(b)). Then, we may evaluate the propagator as (assuming $t > 0$):

$$iG^R(k, t) \approx \sum_{s_M} e^{iks_M} A_M(s_M) \dots \sum_{s_1} e^{iks_1} A_1(s_1), \quad (5)$$

with complexity $O(5M\chi^2)$, χ being the bond dimension.

Exponentiation of influence functional — The problem reduces to compressing A . I can be viewed as a matrix product operator (MPO) that is diagonal in the $\{s\}$ basis, whose virtual space is the phonon Hilbert space. A_0 is an MPS with bond dimension 1. Thus, A can be cast as MPS, too (Fig. 1c). However, since the bond dimension of I is exponentially large, direct compression is infeasible with standard MPS algorithms [43].

In what follows, we show that $I(\{s\})$ can be *exponentiated*, $I(\{s\}) = \exp(\lambda^2 S(\{s\}))$, where $S(\{s\})$ is an diagonal MPO with bond dimension $O(N)$ (Fig. 1d). This fact is central to our compression scheme.

Our key observation is that, viewing $I(\{s\})$ as a controlled evolution sequence for phonon quantum states, the phonons remain in the manifold of coherent states since (a) the unitary operator $U(s)$ preserves coherent state structure, and (b) the initial state $|\phi\rangle$ is a coherent state. We thus write the phonon state as $e^{\lambda^2 S} |\lambda z\rangle$, where S is a complex number and $|\lambda z\rangle = \exp(\sum_q \lambda z_q b_q^\dagger) |\phi\rangle$. z is an N dimensional column vector, whose entry z_q corresponding to the phonon mode with wave vector q . The scaling factors λ, λ^2 are introduced for later convenience.

We derive recursion relations for coherent state parameters S and z . Let $e^{\lambda^2 S_n} |\lambda z_n\rangle = U(s_n) \dots U(s_1) |\phi\rangle$. $U(s_n)$ induces an affine transformation, $(S_n, z_n, 1)^t = B(s_n) (S_{n-1}, z_{n-1}, 1)^t$ [63]. $B(s_n)$ is an $(N+2) \times (N+2)$ matrix. It is independent of λ owing to the rescaling of S and z . The initial condition is $z_0 = 0$ and $S_0 = 0$.

From our definition, $I(\{s\}) = e^{\lambda^2 S_M} \langle 0 | \lambda z_M \rangle = e^{\lambda^2 S_M}$. Using the recursion relation, we cast S_M in matrix product form:

$$I(\{s\}) = e^{\lambda^2 \psi_L B(s_M) \dots B(s_2) B(s_1) \psi_R} \equiv e^{\lambda^2 S(\{s\})}. \quad (6)$$

The boundary vector $\psi_R = (0, 0_{1 \times N}, 1)^t$ encodes the initial condition. $\psi_L = (1, 0_{1 \times N}, 0)$ picks up the value of S_M . Crucially, $S(\{s\})$ has bond dimension $N+2$. Eq. (6) is the key result of this work.

It is interesting to compare Eq. (6) with other equivalent forms. Integrating out phonons in the standard path integral approach also produces $I = \exp(\lambda^2 S)$, where S is given as an algebraic function of $\{s\}$. However, the matrix product structure of S is hidden in this approach.

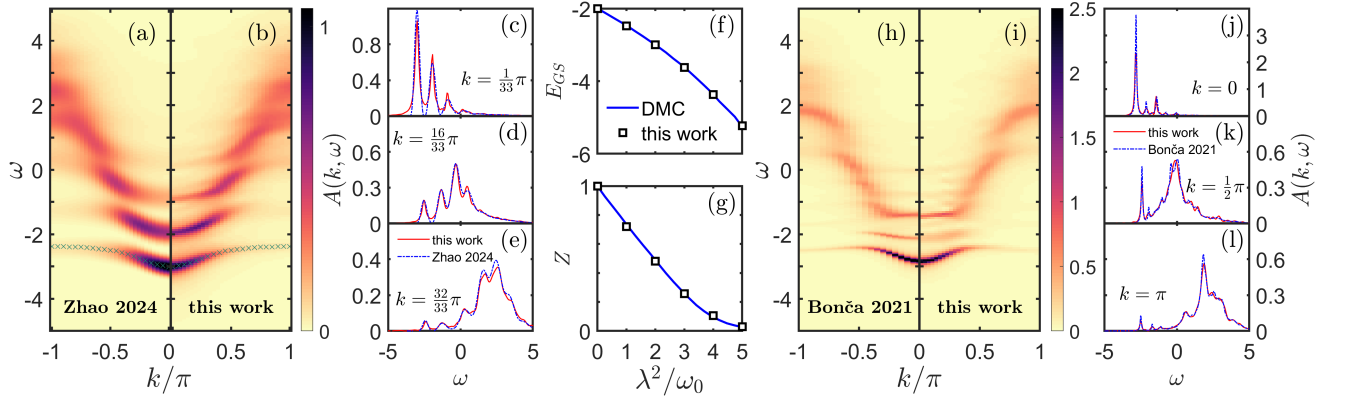


FIG. 2. Polaron spectral function in one dimension. (a)(b) Spectral function $A(k, \omega)$ for the Holstein model $\omega_q = \omega_0 = 1$, $f_q = 1$, and $\lambda = \sqrt{2}$ calculated with system size $N = 16$ and bond dimension $\chi = 120$, compared with the result from MPS Chebyshev expansion [45]. Green crosses mark the dispersion of lowest polaron band from a variational method calculation [40]. (c)(d)(e) Constant- k cuts of $A(k, \omega)$ at representative momenta. (f)(g) Polaron ground state energy E_{GS} and spectral weight Z for the parameter set $\omega_q = \omega_0 = 1$ and $f_q = 1$ extracted from our results, benchmarked against diagrammatic Monte Carlo data [65]. (h)(i) Spectral function for a model with dispersive phonons. $\omega_q = 1 + 0.4 \cos(q)$, $f_q = 1$, and $\lambda = \sqrt[4]{3.36}$, compared with the variational result [42]. (j)(k)(l) Representative constant- k cuts of $A(k, \omega)$.

Compression through flow equation — After exponentiation, the quantum amplitude assumes the form, $A(\{s\}) = e^{\lambda^2 S(\{s\})} A_0(\{s\})$. Differentiating A with respect to λ^2 yields an ordinary differential equation:

$$\frac{dA(\{s\})}{d\lambda^2} = S(\{s\})A(\{s\}). \quad (7)$$

The initial condition is $A(\{s\}) = A_0(\{s\})$ at $\lambda^2 = 0$.

Eq. (7) is a flow equation [66] describing the renormalization of polaron dynamics with increasing electron-phonon coupling. It has the same form as the differential equations that occur in the real/imaginary time evolution of MPS (Fig. 1e). Integrating Eq. (7) by time-dependent variational principle (TDVP) [67, 68] solver with a maximal bond dimension χ results in the compression of A .

Solving Eq. (7) is the most computationally expensive step in our method. It must be solved independently for each time t , which can be parallelized. Once A is compressed, it is then contracted according to Eq. (5). As the momentum k is merely a parameter in the contraction, scanning k over the Brillouin zone does not incur significant computational cost.

Spectral function in one dimension — We compute the spectral function $A(k, \omega) = -\text{Im}G^R(k, \omega)/\pi$, where $G^R(k, \omega)$ is the Fourier transform of $G^R(k, t)$. To this end, we compute $G^R(k, t)$ up to $t_{max} = 80/W$, where W is free electron bandwidth, and then extrapolate it by linear prediction [69, 70]. We use a window function $e^{-\alpha t/t_{max}}$ ($1.4 \leq \alpha \leq 3$) in Fourier transform to suppress spurious peaks. As a result, the spectral peaks are broadened due to the finite energy resolution $\sim 1/t_{max}$. The Trotter time $\epsilon = 0.4/W$.

Fig. 2b shows the spectral function $A(k, \omega)$ for the Holstein model [8] on a chain of $N = 16$ sites, corresponding to the parameter set $\omega_q = \omega_0 = 1$, $f_q = 1$, and

$\lambda = \sqrt{2}$ in Eq. (1). Results for other representative parameters are provided in Ref. 63. The maximal bond dimension $\chi = 120$. The results have converged with respect to both N and χ . We observe idiosyncratic satellite peaks associated with the polaron formation. It can be compared with the result from a previous MPS Chebyshev expansion calculation (Fig. 2a). The lowest polaron band matches quantitatively the variational result [40] (Fig. 2b, green crosses).

Detailed comparison of $A(k, \omega)$ (Fig. 2(c) to (e)) shows quantitative agreement. Small discrepancy in peak width is due to different energy resolutions of these two methods, which are respectively controlled by maximal evolution time t_{max} and the number of Chebyshev moments.

We extract the ground state energy E_G and the spectral weight Z from our data, which correspond respectively to the position and area of the lowest energy spectral peak at $k = 0$ (Fig. 2(f)(g)). We set $\omega_q = \omega_0 = 1$, $f_q = 1$ and vary λ . It is in excellent agreement with the imaginary time diagrammatic Monte Carlo result [65], which attests to the accuracy of our method.

We then turn to models with dispersive phonons. Our method offers considerable flexibility in this regard because the dispersion ω_q enters $S(\{s\})$ as a parameter (Eq. (6)). We set $\omega_q = 1 + 0.4 \cos(q)$ and $\lambda = \sqrt[4]{3.36}$, whereas the other parameters are the same as before. Our results (Fig. 2i) are in good agreement with a previous variational calculation [42] (Fig. 2h). Compared to the Holstein polaron (Fig. 2(a)(b)), the lowest polaron band bends downward near $k = \pm\pi$, mirroring the phonon dispersion.

The spectral line shape from the two methods (Fig. 2(j) to (l)) at representative momenta agree very well, too. The different peak widths again reflect the different en-

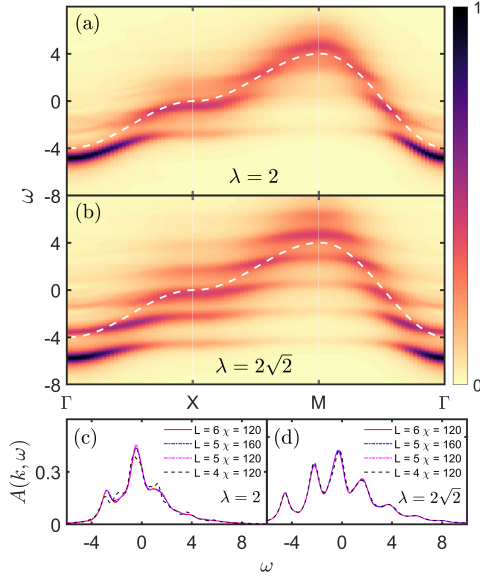


FIG. 3. Polaron spectral function in two-dimensional square lattice. (a) Spectral function $A(k, \omega)$ along high symmetry directions of the first Brillouin zone for the Holstein model $\omega_q = \omega_0 = 2$, $f_q = 1$, $\lambda = 2$. The system size is 6×6 . Bond dimension $\chi = 120$. Dashed line shows the tight binding dispersion. (b) Similar to (a) but for $\lambda = 2\sqrt{2}$. (c)(d) Convergence of the spectral function with respect to the system size and the bond dimension χ at the X point, which we find empirically exhibits the slowest convergence rate.

ergy resolutions. We have also compared the partially integrated spectral weight $\int_{-\infty}^{\omega} A(k, \omega') d\omega'$, which is less sensitive to this issue, and find quantitative agreement for several parameter sets [63].

Spectral function in two dimensions — We turn to the more challenging problem of computing the spectral function in two dimensions, where previous attempts rely on cluster perturbation theory [46, 49]. Going from one dimension to higher dimensions requires minimal modification for our method. The displacement s takes value from the set $\{|\Delta x| \leq 2\} \otimes \{|\Delta y| \leq 2\}$. Both A_0 and S are adjusted accordingly. In practice, we split each variable s_n into Δx_n and Δy_n . This step reduces the physical dimension of MPS at the expense of MPS length.

Fig. 3a shows the spectral function for the Holstein model in two dimensional, $L \times L$ square lattice. We set $\omega_q = \omega_0 = 2$, $f_q = 1$, and $\lambda = 2$. The system size is $L = 6$. The maximal bond dimension $\chi = 120$. We have verified the convergence with respect to both L and χ (Fig. 3(c)). Its features resemble that of the one dimensional model. The spectral weight of the lowest band concentrates near $k = 0$, whereas the weight of higher bands shifts toward the region with larger $|k|$ in momentum space. Dialing up the coupling strength introduces more bands with weaker dispersion (Fig. 3(b)(d)).

Diffusion dynamics — So far our discussion has been dedicated to the spectral function. We now illustrate the

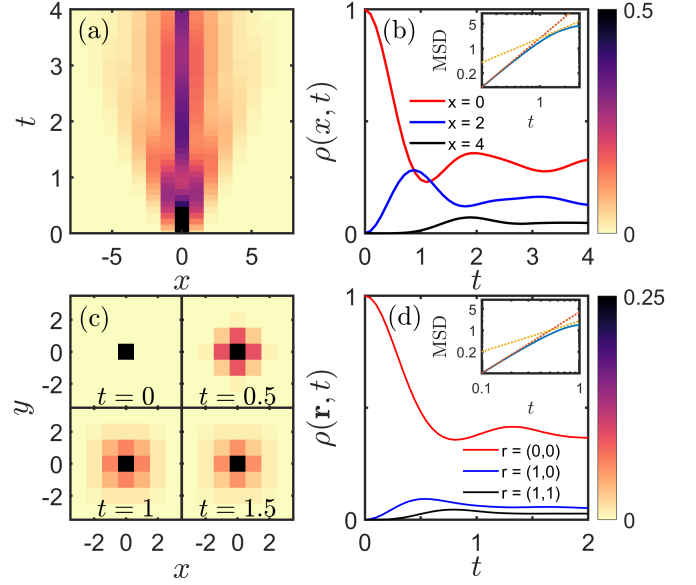


FIG. 4. Polaron diffusion. (a) Electron density $\rho(x, t)$ as a function of coordinate x and time t for the one-dimensional Holstein model. $\omega_q = \omega_0 = 1$, $f_q = 1$, $\lambda = \sqrt{2}$. The system size $N = 15$. Bond dimension $\chi = 300$. (b) Evolution of $\rho(x, t)$ for selected sites. (c) Snapshots of $\rho(x, t)$ at different times for the two-dimensional square lattice Holstein model. $\omega_q = \omega_0 = 2$, $f_q = 1$, $\lambda = 2\sqrt{2}$. We use a 7×7 system with $\chi = 300$. Insets of (b) and (d) show the mean displacement squared (MSD) as a function of time (blue). The ballistic (red) and diffusive (yellow) behaviors are displayed as reference.

versatility of our method by taking a first pass at another category of problems, namely the diffusion dynamics. Specifically, we plant in an empty lattice an electron at the origin, and evolve it according to the Hamiltonian Eq. (1), $|\psi(t)\rangle = e^{-iHt}c_0^\dagger|0\rangle$. We calculate the density $\rho(x, t) = \langle\psi(t)|c_x^\dagger c_x|\psi(t)\rangle$ by using essentially the same method as the propagator [63].

Fig. 4a shows the density evolution for the Holstein model in a chain of 15 sites. We set $\omega_q = \omega_0 = 1$, $f_q = 1$, and $\lambda = \sqrt{2}$. It exhibits oscillatory behavior on top of a diffusion-like spreading (Fig. 4b). The mean displacement squared (MSD) suggests that it moves ballistically at early time and crosses over to diffusive or sub-diffusive behavior at $t \sim 1$ (Fig. 4b, inset). We find similar behavior for the two-dimensional Holstein model on 7×7 square lattice (Fig. 4(c)(d)). The crossover occurs earlier due to the larger bandwidth. Note the MSD is only shown for $t < 1$ in two dimensions because the electron has reached the boundary beyond this point. Longer simulation time and larger system size are needed to clarify the late time behavior of $\rho(x, t)$ for both cases.

Discussion — To summarize, we have shown that the real time Feynman path integral for lattice polaron can be efficiently calculated by compressing the quantum amplitude A as an MPS. The success of this approach relies

on the fact that A indeed admits an MPS representation with low bond dimension. We understand this fact as follows. The virtual space for the *exact* MPS representation of A is the full phonon Hilbert space (Eq. (4b)). Compressing A is amount to searching for a small subspace that captures the dynamics of the system. We construct this space implicitly using the TDVP solution of flow equation (Eq. (7)), whereas the previous variational calculations [36, 37, 40] constructs it explicitly.

Our method paves the way toward a systematic study of polaron dynamics. It can be adapted for Su-Schrieffer-Heeger type models [71, 72] and bipolarons [20, 22]. For the former, a different trotterization scheme is needed for the path integral; for the latter, the physical dimension of the quantum amplitude is doubled. Furthermore, our preliminary analysis has shown that the method could be extended to the case of thermal phonons [73, 74].

Our method exploits the fact that the phonons stay in the coherent state manifold in the time evolution. For Bose polarons [75], it is necessary to extend the manifold to the squeezed coherent states. The influence functional acquires a form different from Eq. (6). Similar reasoning also applies to Fermi polarons [76]. Extending our method to these settings is an open question at the moment. It can be empowered by the tensor cross interpolation method [50–54], thus opening up more possibilities.

We thank Janez Bonča and Shuo Yang for sharing data from Refs. 42 and 45, respectively, and Zi-Xiang Li, Hai-Jun Liao, Tao Shi, Lei Wang, and Tao Xiang for discussions. This work is supported by the National Natural Science Foundation of China (Grants No. 12250008, 12188101), by the National Key Research and Development Program of China (Grants No. 2024YFA1408700, 2021YFA1403800), and the CAS project for Young Scientists in Basic Research (Grant No. YSBR-059).

* yuan.wan@iphy.ac.cn

- [1] T. J. Park and J. C. Light, Unitary quantum time evolution by iterative lanczos reduction, *The Journal of Chemical Physics* **85**, 5870 (1986).
- [2] H. Aoki, N. Tsuji, M. Eckstein, M. Kollar, T. Oka, and P. Werner, Nonequilibrium dynamical mean-field theory and its applications, *Reviews of Modern Physics* **86**, 779 (2014).
- [3] S. Paeckel, T. Köhler, A. Swoboda, S. R. Manmana, U. Schollwöck, and C. Hubig, Time-evolution methods for matrix-product states, *Annals of Physics* **411**, 167998 (2019).
- [4] M. Schmitt and M. Heyl, Quantum many-body dynamics in two dimensions with artificial neural networks, *Physical Review Letters* **125**, 100503 (2020).
- [5] L. D. Landau, Electron motion in crystal lattices, in *Collected Papers of L.D. Landau*, edited by D. ter Haar (Pergamon, 1965) pp. 67–68.
- [6] L. D. Landau and S. I. Pekar, Effective mass of a polaron, *Eksp. Teor. Fiz* **18**, 419 (1948).
- [7] R. P. Feynman, Slow electrons in a polar crystal, *Physical Review* **97**, 660 (1955).
- [8] T. Holstein, Studies of polaron motion, *Annals of Physics* **8**, 325 (1959).
- [9] S. Ciuchi, F. de Pasquale, S. Fratini, and D. Feinberg, Dynamical mean-field theory of the small polaron, *Phys. Rev. B* **56**, 4494 (1997).
- [10] S. Fratini and S. Ciuchi, Dynamical mean-field theory of transport of small polarons, *Phys. Rev. Lett.* **91**, 256403 (2003).
- [11] M. Berciu, Green’s function of a dressed particle, *Physical Review Letters* **97**, 036402 (2006).
- [12] G. L. Goodvin, M. Berciu, and G. A. Sawatzky, Green’s function of the holstein polaron, *Physical Review B* **74**, 245104 (2006).
- [13] B. Pandey and P. B. Littlewood, Going beyond the cumulant approximation: Power series correction to the single-particle green’s function in the holstein system, *Phys. Rev. Lett.* **129**, 136401 (2022).
- [14] P. Mitrić, V. Janković, N. Vukmirović, and D. Tanasković, Spectral Functions of the Holstein Polaron: Exact and Approximate Solutions, *Phys. Rev. Lett.* **129**, 096401 (2022).
- [15] L. Vidmar, J. Bonča, M. Mierzejewski, P. Prelovšek, and S. A. Trugman, Nonequilibrium dynamics of the holstein polaron driven by an external electric field, *Physical Review B* **83**, 134301 (2011).
- [16] D. Golež, J. Bonča, L. Vidmar, and S. A. Trugman, Relaxation dynamics of the holstein polaron, *Phys. Rev. Lett.* **109**, 236402 (2012).
- [17] A. Alexandrov and J. Ranninger, Bipolaronic superconductivity, *Phys. Rev. B* **24**, 1164 (1981).
- [18] A. S. Alexandrov, J. Ranninger, and S. Robaszkiewicz, Bipolaronic superconductivity: Thermodynamics, magnetic properties, and possibility of existence in real substances, *Phys. Rev. B* **33**, 4526 (1986).
- [19] B. K. Chakraverty, J. Ranninger, and D. Feinberg, Experimental and theoretical constraints of bipolaronic superconductivity in hightcmaterials: An impossibility, *Physical Review Letters* **81**, 433 (1998).
- [20] J. Sous, M. Chakraborty, R. V. Krems, and M. Berciu, Light bipolarons stabilized by peierls electron-phonon coupling, *Physical Review Letters* **121**, 247001 (2018).
- [21] J. H. Fetherolf, D. Golež, and T. C. Berkelbach, A unification of the holstein polaron and dynamic disorder pictures of charge transport in organic crystals, *Physical Review X* **10**, 021062 (2020).
- [22] C. Zhang, J. Sous, D. Reichman, M. Berciu, A. Millis, N. Prokof’ev, and B. Svistunov, Bipolaronic high-temperature superconductivity, *Physical Review X* **13**, 011010 (2023).
- [23] X.-Y. Zhu and V. Podzorov, Charge carriers in hybrid organic–inorganic lead halide perovskites might be protected as large polarons, *The Journal of Physical Chemistry Letters* **6**, 4758 (2015).
- [24] H. Zhu, K. Miyata, Y. Fu, J. Wang, P. P. Joshi, D. Niesner, K. W. Williams, S. Jin, and X.-Y. Zhu, Screening in crystalline liquids protects energetic carriers in hybrid perovskites, *Science* **353**, 1409 (2016).
- [25] Y. Fu, H. Zhu, J. Chen, M. P. Hautzinger, X.-Y. Zhu, and S. Jin, Metal halide perovskite nanostructures for optoelectronic applications and the study of physical properties, *Nature Reviews Materials* **4**, 169 (2019).

- [26] D. Ghosh, E. Welch, A. J. Neukirch, A. Zakhidov, and S. Tretiak, Polarons in halide perovskites: A perspective, *The Journal of Physical Chemistry Letters* **11**, 3271 (2020).
- [27] A. S. Alexandrov and J. T. Devreese, *Advances in Polaron Physics* (Springer Berlin Heidelberg, 2010).
- [28] E. Y. Loh, J. E. Gubernatis, R. T. Scalettar, S. R. White, D. J. Scalapino, and R. L. Sugar, Sign problem in the numerical simulation of many-electron systems, *Physical Review B* **41**, 9301 (1990).
- [29] G. Cohen, E. Gull, D. R. Reichman, and A. J. Millis, Taming the dynamical sign problem in real-time evolution of quantum many-body problems, *Physical Review Letters* **115**, 266802 (2015).
- [30] N. V. Prokof'ev and B. V. Svistunov, Polaron problem by diagrammatic quantum monte carlo, *Phys. Rev. Lett.* **81**, 2514 (1998).
- [31] A. Mishchenko, N. Prokof'ev, A. Sakamoto, and B. Svistunov, Diagrammatic quantum monte carlo study of the fröhlich polaron, *Physical Review B* **62**, 6317 (2000).
- [32] A. S. Mishchenko, N. Nagaosa, N. V. Prokof'ev, A. Sakamoto, and B. V. Svistunov, Optical conductivity of the fröhlich polaron, *Phys. Rev. Lett.* **91**, 236401 (2003).
- [33] G. De Filippis, V. Cataudella, A. S. Mishchenko, C. A. Perroni, and J. T. Devreese, Validity of the franck-condon principle in the optical spectroscopy: Optical conductivity of the fröhlich polaron, *Phys. Rev. Lett.* **96**, 136405 (2006).
- [34] G. L. Goodvin, A. S. Mishchenko, and M. Berciu, Optical conductivity of the holstein polaron, *Physical Review Letters* **107**, 076403 (2011).
- [35] A. Mishchenko, N. Nagaosa, G. De Filippis, A. de Candia, and V. Cataudella, Mobility of holstein polaron at finite temperature: An unbiased approach, *Physical Review Letters* **114**, 146401 (2015).
- [36] A. H. Romero, D. W. Brown, and K. Lindenberg, Converging toward a practical solution of the holstein molecular crystal model, *The Journal of Chemical Physics* **109**, 6540 (1998).
- [37] G. Wellein and H. Fehske, Self-trapping problem of electrons or excitons in one dimension, *Physical Review B* **58**, 6208 (1998).
- [38] C. Zhang, E. Jeckelmann, and S. R. White, Density matrix approach to local hilbert space reduction, *Physical Review Letters* **80**, 2661 (1998).
- [39] C. Zhang, E. Jeckelmann, and S. R. White, Dynamical properties of the one-dimensional holstein model, *Physical Review B* **60**, 14092 (1999).
- [40] J. Bonča, S. A. Trugman, and I. Batistić, Holstein polaron, *Physical Review B* **60**, 1633 (1999).
- [41] P. E. Dolgirev, Y.-F. Qu, M. B. Zvonarev, T. Shi, and E. Demler, Emergence of a sharp quantum collective mode in a one-dimensional fermi polaron, *Physical Review X* **11**, 041015 (2021).
- [42] J. Bonča and S. A. Trugman, Dynamic properties of a polaron coupled to dispersive optical phonons, *Physical Review B* **103**, 054304 (2021).
- [43] U. Schollwöck, The density-matrix renormalization group in the age of matrix product states, *Annals of Physics* **326**, 96 (2011), january 2011 Special Issue.
- [44] E. Jeckelmann and S. R. White, Density-matrix renormalization-group study of the polaron problem in the holstein model, *Physical Review B* **57**, 6376 (1998).
- [45] P.-Y. Zhao, K. Ding, and S. Yang, Chebyshev pseudosite matrix product state approach for the spectral functions of electron-phonon coupling systems, *Physical Review Research* **5**, 023026 (2023).
- [46] M. Hohenadler, M. Aichhorn, and W. von der Linden, Spectral function of electron-phonon models by cluster perturbation theory, *Physical Review B* **68**, 184304 (2003).
- [47] Y. Ashida, T. Shi, M. C. Bañuls, J. I. Cirac, and E. Demler, Solving quantum impurity problems in and out of equilibrium with the variational approach, *Phys. Rev. Lett.* **121**, 026805 (2018).
- [48] T. Shi, E. Demler, and J. Ignacio Cirac, Variational study of fermionic and bosonic systems with non-gaussian states: Theory and applications, *Annals of Physics* **390**, 245 (2018).
- [49] P.-Y. Zhao, K. Ding, and S. Yang, Chebyshev pseudosite matrix product state approach for cluster perturbation theory (2024).
- [50] I. Oseledets and E. Tyrtysnikov, Tt-cross approximation for multidimensional arrays, *Linear Algebra and its Applications* **432**, 70 (2010).
- [51] I. V. Oseledets, Tensor-train decomposition, *SIAM Journal on Scientific Computing* **33**, 2295 (2011).
- [52] S. Dolgov and D. Savostyanov, Parallel cross interpolation for high-precision calculation of high-dimensional integrals, *Computer Physics Communications* **246**, 106869 (2020).
- [53] Y. Núñez Fernández, M. Jeannin, P. T. Dumitrescu, T. Kloss, J. Kaye, O. Parcollet, and X. Waintal, Learning feynman diagrams with tensor trains, *Physical Review X* **12**, 041018 (2022).
- [54] Y. Núñez Fernández, M. K. Ritter, M. Jeannin, J.-W. Li, T. Kloss, T. Louvet, S. Terasaki, O. Parcollet, J. von Delft, H. Shinaoka, and X. Waintal, Learning tensor networks with tensor cross interpolation: New algorithms and libraries, *SciPost Physics* **18**, 10.21468/scipostphys.18.3.104 (2025).
- [55] A. Strathearn, P. Kirtan, D. Kilda, J. Keeling, and B. W. Lovett, Efficient non-markovian quantum dynamics using time-evolving matrix product operators, *Nature Communications* **9**, 10.1038/s41467-018-05617-3 (2018).
- [56] M. R. Jørgensen and F. A. Pollock, Exploiting the causal tensor network structure of quantum processes to efficiently simulate non-markovian path integrals, *Physical Review Letters* **123**, 240602 (2019).
- [57] M. Cygorek, M. Cosacchi, A. Vagov, V. M. Axt, B. W. Lovett, J. Keeling, and E. M. Gauger, Simulation of open quantum systems by automated compression of arbitrary environments, *Nature Physics* **18**, 662 (2022).
- [58] M. C. Bañuls, M. B. Hastings, F. Verstraete, and J. I. Cirac, Matrix product states for dynamical simulation of infinite chains, *Physical Review Letters* **102**, 240603 (2009).
- [59] Y.-K. Huang, P. Chen, Y.-J. Kao, and T. Xiang, Long-time dynamics of quantum chains: Transfer-matrix renormalization group and entanglement of the maximal eigenvector, *Physical Review B* **89**, 201102 (2014).
- [60] A. Lerose, M. Sonner, and D. A. Abanin, Influence matrix approach to many-body floquet dynamics, *Physical Review X* **11**, 021040 (2021).
- [61] G. E. Fux, D. Kilda, B. W. Lovett, and J. Keeling, Tensor network simulation of chains of non-markovian open quantum systems, *Physical Review Research* **5**, 033078 (2023).

- (2023).
- [62] D. J. J. Marchand and M. Berciu, Effect of dispersive optical phonons on the behavior of a holstein polaron, *Physical Review B* **88**, 060301 (2013).
 - [63] Supplemental material.
 - [64] T. D. Lee, F. E. Low, and D. Pines, The motion of slow electrons in a polar crystal, *Physical Review* **90**, 297 (1953).
 - [65] S. Ragni, *Diagrammatic Monte Carlo study of the Holstein polaron*, Master's thesis, University of Bologna, School of Science, Department of Physics and Astronomy (2020).
 - [66] F. Wegner, Flow-equations for hamiltonians, *Annalen der Physik* **506**, 77 (1994).
 - [67] J. Haegeman, J. I. Cirac, T. J. Osborne, I. Pižorn, H. Verschelde, and F. Verstraete, Time-dependent variational principle for quantum lattices, *Physical Review Letters* **107**, 070601 (2011).
 - [68] J. Haegeman, C. Lubich, I. Oseledets, B. Vandereycken, and F. Verstraete, Unifying time evolution and optimization with matrix product states, *Physical Review B* **94**, 165116 (2016).
 - [69] S. R. White and I. Affleck, Spectral function for the $S = 1$ Heisenberg antiferromagnetic chain, *Physical Review B* **77**, 134437 (2008).
 - [70] T. Barthel, U. Schollwöck, and S. R. White, Spectral functions in one-dimensional quantum systems at finite temperature using the density matrix renormalization group, *Physical Review B* **79**, 245101 (2009).
 - [71] M. Capone, W. Stephan, and M. Grilli, Small-polaron formation and optical absorption in su-schrieffer-heeger and holstein models, *Phys. Rev. B* **56**, 4484 (1997).
 - [72] D. J. J. Marchand, G. De Filippis, V. Cataudella, M. Berciu, N. Nagaosa, N. V. Prokof'ev, A. S. Mishchenko, and P. C. E. Stamp, Sharp transition for single polarons in the one-dimensional su-schrieffer-heeger model, *Physical Review Letters* **105**, 266605 (2010).
 - [73] J. Bonča, S. A. Trugman, and M. Berciu, Spectral function of the holstein polaron at finite temperature, *Physical Review B* **100**, 094307 (2019).
 - [74] D. Jansen, J. Bonča, and F. Heidrich-Meisner, Finite-temperature density-matrix renormalization group method for electron-phonon systems: Thermodynamics and holstein-polaron spectral functions, *Physical Review B* **102**, 165155 (2020).
 - [75] F. Grusdt, N. Mostaan, E. Demler, and L. A. P. Ardila, Impurities and polarons in bosonic quantum gases: a review on recent progress (2024), arXiv:2410.09413 [cond-mat.quant-gas].
 - [76] P. Massignan, M. Zaccanti, and G. M. Bruun, Polarons, dressed molecules and itinerant ferromagnetism in ultracold fermi gases, *Reports on Progress in Physics* **77**, 034401 (2014).

Appendix A: Path integral representation of polaron propagator

In this section, we fill in the gaps in the derivation of the path integral representation of electron propagator. We consider a chain of N sites subject to periodic boundary condition. The Hamiltonian reads:

$$H = - \underbrace{\sum_i (c_i^\dagger c_{i+1} + c_{i+1}^\dagger c_i)}_K + \underbrace{\sum_q \omega_q b_q^\dagger b_q - \lambda f_q n_q (b_q + b_{-q}^\dagger)}_V. \quad (\text{A.1})$$

The first term K is the electron kinetic energy. c_i^\dagger (c_i) creates (annihilates) a spinless electron on site i . We set the electron hopping amplitude to 1 by rescaling the unit of energy. The second term V describes the phonons and their coupling to electron. b_q^\dagger (b_q) creates (annihilates) a phonon with wave vector q . $n_q = \frac{1}{\sqrt{N}} \sum_k c_{k+q}^\dagger c_k$ is the Fourier transform of electron density operator. ω_q is the phonon dispersion relation. $f_q = f_{-q}^*$ is a form factor. $\lambda > 0$ is the electron-phonon coupling constant.

We are interested in the zero temperature electron propagator in the momentum space:

$$iG^R(k, t) = \theta(t) \langle 0 | c_k(t) c_k^\dagger(0) | 0 \rangle = \langle 0 | c_k e^{-iHt} c_k^\dagger | 0 \rangle. \quad (\text{A.2})$$

$|0\rangle$ refers to the ground state of Eq. (A.1) in the zero-electron sector. As c_k^\dagger creates an electron, the ensuing time evolution occurs in the one-electron sector.

To derive the path integral representation, we use the second order Suzuki-Trotter decomposition, $e^{-i\epsilon H} = e^{-i\frac{\epsilon}{2}V} e^{-i\epsilon K} e^{-i\frac{\epsilon}{2}V} + O(\epsilon^3)$. Substituting it into the expression for G^R , we obtain:

$$iG^R(k, t) = \theta(t) \sum_r e^{ikr} \langle 0 | c_r \underbrace{e^{-i\frac{\epsilon}{2}V} e^{-i\epsilon K} e^{-i\epsilon V} \dots e^{-i\epsilon V} e^{-i\epsilon K} e^{-i\frac{\epsilon}{2}V}}_{M \text{ hopping terms}} c_0^\dagger | 0 \rangle. \quad (\text{A.3})$$

We insert the resolution of identity by electron position eigenstates and use the fact that V commutes with the electron position operator:

$$iG^R(k, t) = \theta(t) \sum_{\{x\}} e^{ikr} \langle x_M | e^{-i\epsilon K} | x_{M-1} \rangle \dots \langle x_1 | e^{-i\epsilon K} | x_0 \rangle \langle \phi | e^{-i\frac{\epsilon}{2}V(x_M)} e^{-iV(x_{M-1})} \dots e^{-i\epsilon V(x_1)} e^{-i\frac{\epsilon}{2}V(x_0)} | \phi \rangle. \quad (\text{A.4})$$

The summation is over all electron paths x_0, x_1, \dots, x_M , with the boundary condition $x_0 = 0$ and $x_M = r$. $V(x)$ refers to the phonon Hamiltonian when the electron is at position x :

$$V(x) = \sum_q (\omega_q b_q^\dagger b_q - \frac{\lambda f_q e^{iqx}}{\sqrt{N}} b_q - \frac{\lambda f_q^* e^{-iqx}}{\sqrt{N}} b_q^\dagger). \quad (\text{A.5})$$

Here, we have used $n_q |x\rangle = \frac{1}{\sqrt{N}} e^{iqx} |x\rangle$. $|\phi\rangle$ is the phonon vacuum.

In the next step, we perform a change of variable from electron position x_n to electron displacement $s_n = x_n - x_{n-1}$:

$$iG^R(k, t) = \theta(t) \sum_{\{s\}} \left(\prod_{j=1}^M e^{iks_j} \right) A_0(\{s\}) I(\{s\}). \quad (\text{A.6})$$

Here, $\{s\} = \{s_M, \dots, s_2, s_1\}$. A_0 is the quantum amplitude for a free particle:

$$A_0(\{s\}) = \prod_{j=1}^M f(s_j), \quad f(s) = \langle x + s | e^{-i\epsilon K} | x \rangle = \begin{cases} 1 - \epsilon^2 & (s = 0) \\ i\epsilon & (s = \pm 1) \\ -\epsilon^2/2 & (s = \pm 2) \end{cases}. \quad (\text{A.7})$$

Here, we have truncated the range of s to $|s| \leq 2$. This truncation introduces an error of order ϵ^3 , which is comparable to that of the Trotter error. The phonon influence functional I is given by:

$$I(\{s\}) = \langle \phi | e^{-i\frac{\epsilon}{2}V(x_M)} e^{-i\epsilon V(x_{M-1})} \dots e^{-i\epsilon V(x_1)} e^{-i\frac{\epsilon}{2}V(x_0)} | \phi \rangle. \quad (\text{A.8})$$

The right hand side depends on $\{s\}$ implicitly through the relation $x_j = x_{j-1} + s_j$, with the initial condition $x_0 = 0$.

We wish to make the dependence of I on $\{s\}$ explicit. To this end, we use the translation operator $T(x)$ on phonon states $T(-x)b_qT(x) = e^{-iqx}b_q$. It follows that $T(x)V(0)T(-x) = V(x)$. I now depends on $\{s\}$ explicitly:

$$\begin{aligned} I(\{s\}) &= \langle \phi | e^{-i\frac{\epsilon}{2}V(0)} T(-s_M) e^{-i\epsilon V(0)} \cdots T(-s_2) e^{-i\epsilon V(0)} T(-s_1) e^{-i\frac{\epsilon}{2}V(0)} | \phi \rangle \\ &= \langle \phi | U(s_M) \cdots U(s_2) U(s_1) | \phi \rangle. \end{aligned} \quad (\text{A.9})$$

Here, we have defined the unitary operator:

$$U(s) = e^{-i\frac{\epsilon}{2}V(0)} T(-s) e^{-i\frac{\epsilon}{2}V(0)}. \quad (\text{A.10})$$

Appendix B: Exponentiation of influence functional

$I(\{s\})$ already has a matrix product structure; it can be viewed as a diagonal matrix product operator whose virtual space is the phonon Hilbert space. In this section, we show that $I(\{s\})$ can be exponentiated as:

$$I(\{s\}) = e^{\lambda^2 S(\{s\})}, \quad (\text{B.1})$$

where $S(\{s\})$ has a matrix product form whose bond dimension is $N + 2$.

We view $I(\{s\})$ as a sequence of controlled unitary evolution of the phonon states, starting from the phonon vacuum $|\phi\rangle$. We note that $U(s)$ maps phonon coherent state to coherent state, and, furthermore, that the initial state is a coherent state. Therefore, the phonons stay in the coherent state manifold. We may parametrize the phonon state as:

$$e^{\lambda^2 S_j} |\lambda z_j\rangle = U(s_j) \cdots U(s_2) U(s_1) |\phi\rangle. \quad (\text{B.2})$$

Here, S_j is a complex number; z_j is a N -dimensional complex vector that parametrize the coherent state, whose entry runs over all phonon wave vectors. In particular, z_q corresponds to the phonon mode with wave vector q . The scaling factor λ^2 (λ) in front of S_j (z_j) is for later convenience.

We now derive a recursion relation for the parameters S_j and z_j . We first consider the action of $\exp(-i\frac{\epsilon}{2}V(0))$ on phonon coherent state:

$$e^{-i\frac{\epsilon}{2}V(0)} |\lambda z\rangle = \prod_q^{\otimes} \exp(-i\frac{\omega_q \epsilon}{2} b_q^\dagger b_q + i\frac{\lambda f_q \epsilon}{2\sqrt{N}} b_q + i\frac{\lambda f_q^* \epsilon}{2\sqrt{N}} b_q^\dagger) |\lambda z_q\rangle. \quad (\text{B.3})$$

We untangle the operator exponential by the following identity:

$$e^{-Ab^\dagger b + Bb + Cb^\dagger} = e^{\frac{BC}{A} - \frac{BC}{A^2}(1-e^{-A})} e^{-Ab^\dagger b} e^{C\frac{e^A-1}{A}b^\dagger} e^{B\frac{1-e^{-A}}{A}b}. \quad (\text{B.4})$$

Setting

$$A = \frac{i\omega_q \epsilon}{2}; \quad B = i\frac{\lambda f_q \epsilon}{2\sqrt{N}}; \quad C = i\frac{\lambda f_q^* \epsilon}{2\sqrt{N}}, \quad (\text{B.5})$$

we obtain:

$$\begin{aligned} \exp(-i\frac{\omega_q \epsilon}{2} b_q^\dagger b_q + i\frac{\lambda f_q \epsilon}{2\sqrt{N}} b_q + i\frac{\lambda f_q^* \epsilon}{2\sqrt{N}} b_q^\dagger) &= \exp[i\frac{\lambda^2 |f_q|^2}{2N\omega_q} \epsilon - \frac{\lambda^2 |f_q|^2}{N\omega_q^2} (1 - e^{-i\frac{\omega_q \epsilon}{2}})] \\ &\exp(-i\frac{\omega_q \epsilon}{2} b_q^\dagger b_q) \exp[\frac{\lambda f_q^*}{\sqrt{N}\omega_q} (e^{i\frac{\omega_q \epsilon}{2}} - 1) b_q^\dagger] \exp[\frac{\lambda f_q}{\sqrt{N}\omega_q} (1 - e^{-i\frac{\omega_q \epsilon}{2}}) b_q]. \end{aligned} \quad (\text{B.6})$$

Computing its action on coherent state is now straightforward:

$$\begin{aligned} \exp(-i\frac{\omega_q \epsilon}{2} b_q^\dagger b_q + i\frac{\lambda f_q \epsilon}{2\sqrt{N}} b_q + i\frac{\lambda f_q^* \epsilon}{2\sqrt{N}} b_q^\dagger) |\lambda z_q\rangle &= \exp[i\frac{\lambda^2 |f_q|^2}{2N\omega_q} \epsilon - \frac{\lambda^2 |f_q|^2}{N\omega_q^2} (1 - e^{-i\frac{\omega_q \epsilon}{2}}) + \frac{\lambda^2 f_q}{\sqrt{N}\omega_q} (1 - e^{-i\frac{\omega_q \epsilon}{2}}) z_q] \\ &|\lambda e^{-i\frac{\omega_q \epsilon}{2}} z_q + \frac{\lambda f_q^*}{\sqrt{N}\omega_q} (1 - e^{-i\frac{\omega_q \epsilon}{2}})\rangle. \end{aligned} \quad (\text{B.7})$$

Collecting the results for different q , we obtain:

$$e^{-i\frac{\epsilon}{2}V(0)}e^{\lambda^2 S}|\lambda z\rangle = e^{\lambda^2(S+c+\beta^\dagger z)}|\lambda(\mathcal{V}z + \alpha)\rangle, \quad (\text{B.8})$$

Here, \mathcal{V} is a diagonal matrix whose diagonal entry reads:

$$\mathcal{V}_{qq} = \exp(-i\frac{\omega_q \epsilon}{2}). \quad (\text{B.9a})$$

α and β are complex N -dimensional vectors:

$$\alpha_q = \frac{f_q^*}{\sqrt{N}\omega_q}(1 - e^{-i\frac{\omega_q \epsilon}{2}}); \quad \beta_q = \frac{f_q^*}{\sqrt{N}\omega_q}(1 - e^{i\frac{\omega_q \epsilon}{2}}) = -(\mathcal{V}^\dagger \alpha)_q; \quad (\text{B.9b})$$

c is a complex number:

$$c = \frac{1}{N} \sum_q \frac{|f_q|^2}{\omega_q} (i\frac{\epsilon}{2} - \frac{1 - e^{-i\frac{\omega_q \epsilon}{2}}}{\omega_q}). \quad (\text{B.9c})$$

We recognize that the action of $\exp(-i\frac{\epsilon}{2}V(0))$ on phonon coherent state in fact induces an affine transformation:

$$S \xrightarrow{e^{-i\frac{\epsilon}{2}V(0)}} S + c + \beta^\dagger z, \quad z \xrightarrow{e^{-i\frac{\epsilon}{2}V(0)}} \mathcal{V}z + \alpha. \quad (\text{B.10})$$

We recast the above in matrix form:

$$\begin{pmatrix} S \\ z \\ 1 \end{pmatrix} \xrightarrow{e^{-i\frac{\epsilon}{2}V(0)}} \begin{pmatrix} 1 & \beta^\dagger & c \\ 0 & \mathcal{V} & \alpha \\ 0 & 0 & 1 \end{pmatrix} \begin{pmatrix} S \\ z \\ 1 \end{pmatrix}. \quad (\text{B.11})$$

Likewise, the lattice translation operator $T(x)$ maps coherent state to coherent state. To prove this, we use:

$$T(x)^{-1}b_q T(x) = e^{-iqx}b_q. \quad (\text{B.12})$$

It follows that:

$$b_q(T(x)|z_q\rangle) = e^{-iqx}z_q T(x)|z_q\rangle, \quad (\text{B.13})$$

which implies

$$T(x)|z_q\rangle = |e^{-iqx}z_q\rangle. \quad (\text{B.14})$$

Collecting the results for different q , we find:

$$T(-s)e^{\lambda^2 S}|\lambda z\rangle = e^{\lambda^2 S}|\lambda \mathcal{T}(-s)z\rangle, \quad (\text{B.15})$$

where $\mathcal{T}(x)$ is a diagonal unitary matrix whose diagonal entries are given by:

$$\mathcal{T}(x)_{qq} = e^{-iqx}. \quad (\text{B.16})$$

The induced linear transformation on S and z can be written in matrix form:

$$\begin{pmatrix} S \\ z \\ 1 \end{pmatrix} \xrightarrow{T(-s)} \begin{pmatrix} 1 & 0 & 0 \\ 0 & \mathcal{T}(-s) & 0 \\ 0 & 0 & 1 \end{pmatrix} \begin{pmatrix} S \\ z \\ 1 \end{pmatrix}. \quad (\text{B.17})$$

Combining the above results, we arrive at the following recursion relation for S_j and z_j :

$$\begin{pmatrix} S_j \\ z_j \\ 1 \end{pmatrix} = \begin{pmatrix} 1 & \beta^\dagger & c \\ 0 & \mathcal{V} & \alpha \\ 0 & 0 & 1 \end{pmatrix} \begin{pmatrix} 1 & 0 & 0 \\ 0 & \mathcal{T}(-s_j) & 0 \\ 0 & 0 & 1 \end{pmatrix} \begin{pmatrix} 1 & \beta^\dagger & c \\ 0 & \mathcal{V} & \alpha \\ 0 & 0 & 1 \end{pmatrix} \begin{pmatrix} S_{j-1} \\ z_{j-1} \\ 1 \end{pmatrix} \equiv B(s_j) \begin{pmatrix} S_{j-1} \\ z_{j-1} \\ 1 \end{pmatrix}. \quad (\text{B.18})$$

Here, $B(s_j)$ is a $N + 2$ dimensional square matrix. The initial condition is $z_0 = 0$ and $S_0 = 0$.

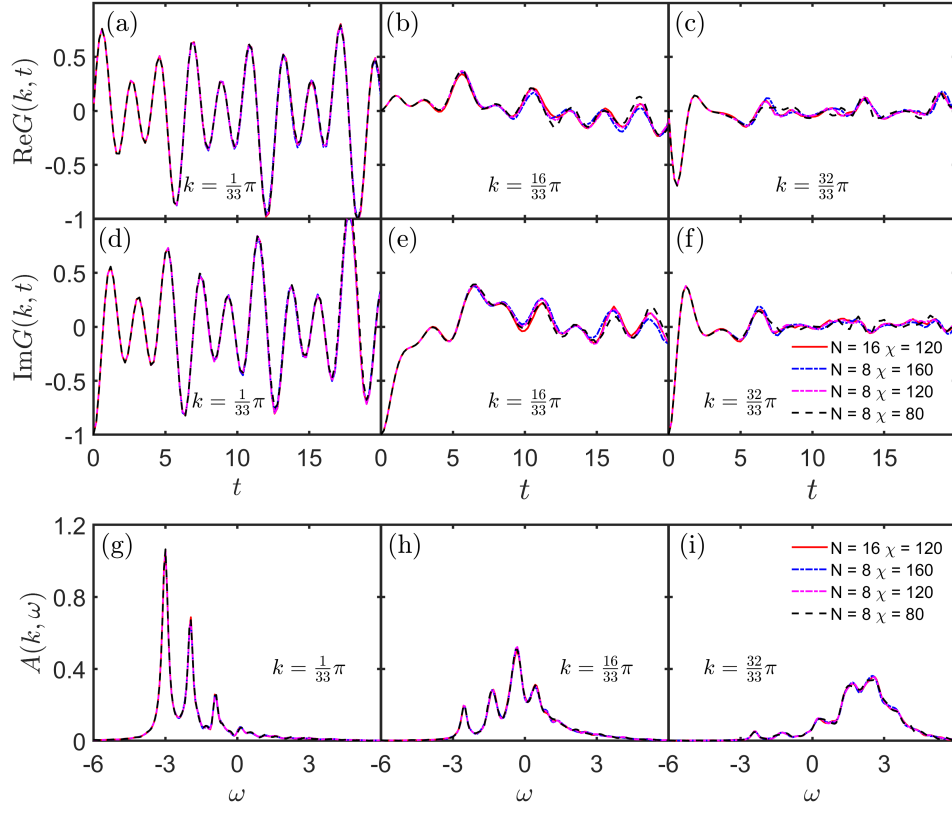


FIG. C.1. Top rows: the real (a~c) and imaginary (d~f) part of the electron propagator of the one dimensional Holstein model at three representative wave vectors. The parameters are: $\omega_q = \omega_0 = 1$, $\lambda = \sqrt{2}$, and $f_q = 1$. Bottom row: the corresponding spectral function ($g \sim i$). Data for different system sizes N and bond dimensions χ are shown.

We now compute $I(\{s\})$ using the recursion relation. By definition:

$$I(\{s\}) = e^{\lambda^2 S_M} \langle 0 | \lambda z_M \rangle = e^{\lambda^2 S_M}. \quad (\text{B.19})$$

S_M can be found by using the iteration relation:

$$S_M = \psi_L B(s_M) \cdots B(s_2) B(s_1) \psi_R; \quad \psi_L = \begin{pmatrix} 1 & 0 & 0 \end{pmatrix}; \quad \psi_R = \begin{pmatrix} 0 \\ 0 \\ 1 \end{pmatrix}. \quad (\text{B.20})$$

We see that S_M is expressed in matrix product form; the bond dimension is $N + 2$. Note all the entries in B are independent of λ thanks to the scaling factor introduced in the definition of z and S .

Appendix C: Spectral function of one-dimensional Holstein model

Fig. C.1 shows the data for the electron propagator $G^R(k, t)$ in the time domain at three representative wave vectors. Note these wave vectors are identical to what are shown in Figure 2c~e in the main text. Both the real (panels a~c) and the imaginary parts (panels d~f) are shown. We find that $G^R(k, t)$ at $k \approx 0$ reaches convergence already at low bond dimension $\chi = 80$ and small system size $N = 8$. By contrast, $G^R(k, t)$ at $k \approx \pi/2$ and $k \approx \pi$ exhibit slower rate of convergence.

An interesting feature of the time domain data is that the data at different times exhibit a relatively uniform rate of convergence with respect to χ . We do observe a moderate difference, though. $G^R(k, t)$ at early time and some late time intervals reaches convergence relatively early (at $\chi = 80$), whereas, for some specific intervals, there is a discernible difference between data at $\chi = 120$ and $\chi = 160$, indicating that the data at these times have not yet reached full convergence but are fairly close to it.

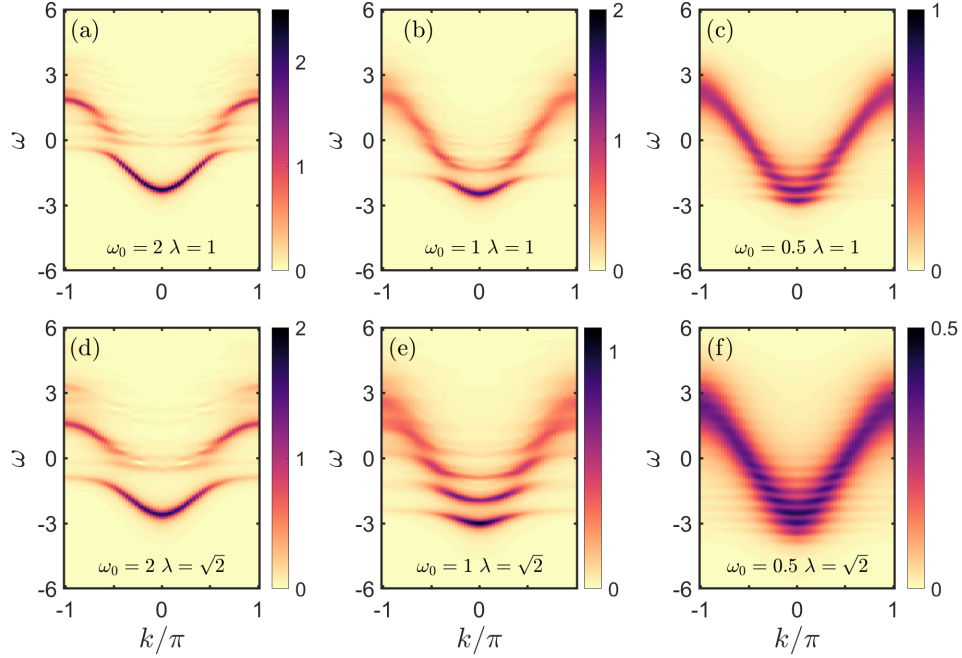


FIG. C.2. Spectral function of one dimension Holstein model. We set $\omega_q = \omega_0$ and $f_q = 1$. The system size $N = 16$. Maximal bond dimension $\chi = 120$.

The nearly uniform convergence for different times is due to the fact that the physical time corresponds to the length direction of the MPS. It proves advantageous for computing spectral functions (panel g~i). We find that the spectral functions in fact converge much faster than the time domain data. This behavior is expected: the spectral function at low frequencies are insensitive to small, local changes in the time domain data.

Fig. C.2 shows the spectral function of the one-dimensional Holstein model for a few representative parameter sets. We set $\omega_q = \omega_0$ and $f_q = 1$. The system size $N = 16$. The maximal bond dimension $\chi = 120$. The top row (panel a~c) show the result for $\lambda = 1$ with increasingly softer phonon frequency. The bottom row (panel d~f) is similar but with stronger coupling constant $\lambda = \sqrt{2}$. The overall trend is that increasing λ and/or decreasing ω_0 introduce more satellite peaks, reflecting the fact that the combination λ^2/ω_0 controls the effective coupling strength. Interestingly, we find that, for $\omega_0 = 2$, we observe shadow bands with relative small spectral weight between the main bands. We have verified that these are not artifacts. The microscopic origin of these shadow bands are not entirely clear at the moment.

Appendix D: Spectral function for dispersive model

Fig. D.1 shows the spectral function for a one-dimensional model with dispersive phonons. Following Ref. 42, we set $\omega_q = 1 + 2t_{ph} \cos q$, $f_q = 1$, and $\lambda = (4 - 16t_{ph}^2)^{1/4}$. We use a system of $N = 16$ sites. The maximal bond dimension $\chi = 120$. We find that our results agree well with that of Ref. 42, which uses a variational construction of low-energy eigenstates. Compared with dispersionless phonons ($t_{ph} = 0$), the satellite peaks for the case of dispersive phonons ($t_{ph} = \pm 0.2$) show narrower spacing in energy. This feature reflects the fact that the phonon frequency minimum $\omega_{min} = 1 - 2|t_{ph}| = 0.6$ is smaller than the dispersionless case. For $t_{ph} = -0.2$ ($t_{ph} = 0.2$), the lowest polaron band bends upward (downward) near the Brillouin zone boundary, mirroring the phonon dispersion.

We carry out a quantitative comparison of our results with that of Ref. 42 in Fig. D.2. We find good agreement between the two methods. We note that the spectral peaks from Ref. 42 have smaller peak width than ours. This difference is due to the different energy resolution. In the former method, a spectral broadening factor is used, whereas, in the latter, the energy resolution is controlled by the maximal time of evolution.

We therefore compare the partially integrated spectral function $\int_{-\infty}^{\omega} A(k, \omega') d\omega'$. This object is less sensitive to the energy resolution. The steps of the partially integrated spectral function correspond to peaks in $A(k, \omega)$. Fig. D.3 shows the comparison of the partially integrate spectral function, which shows quantitative agreement between the two methods.

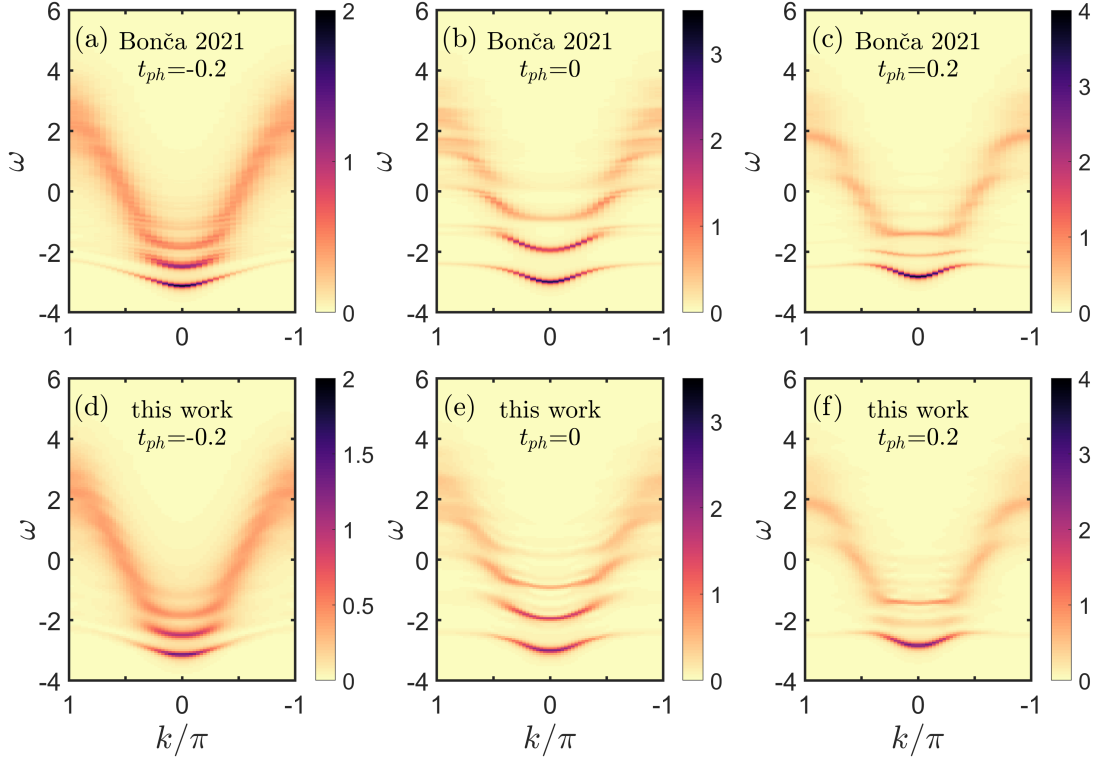


FIG. D.1. Spectral function of one dimension model with dispersive phonons. We set $\omega_q = 1 + 2t_{ph} \cos q$, $f_q = 1$, and $\lambda = (4 - 16t_{ph}^2)^{1/4}$. The system size $N = 16$. The maximal bond dimension $\chi = 120$. The top row is reproduced from a previous variational calculation [42], where the bottom row is from this work.

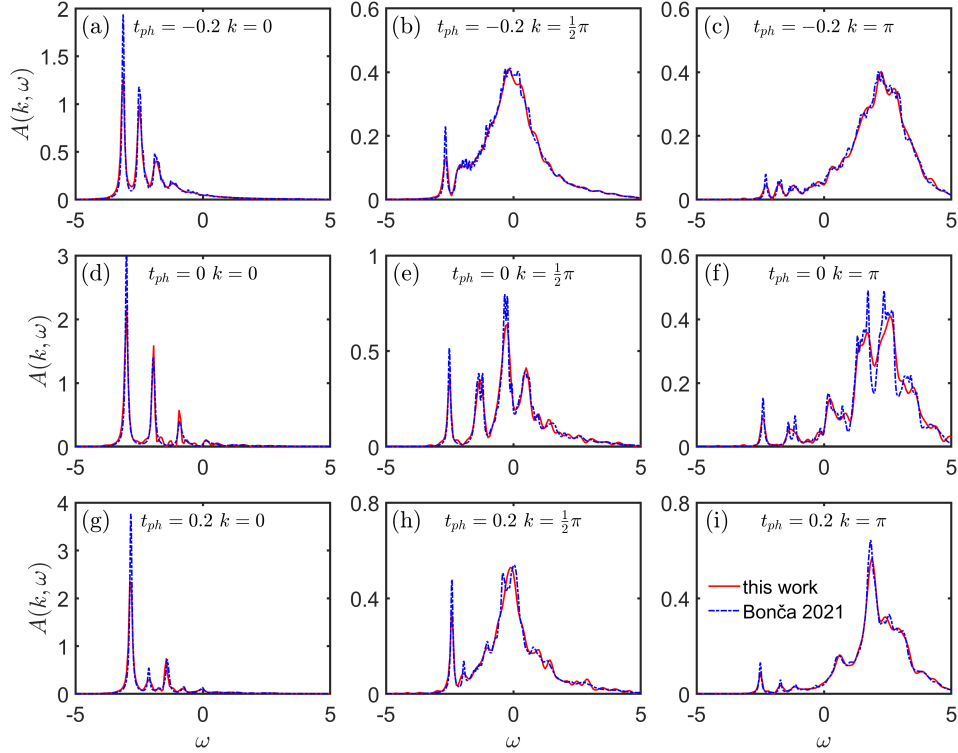


FIG. D.2. Constant k -cuts of the spectral function $A(k, \omega)$ for three representative wave vectors $k = 0, \pi/2$, and π . The parameter choice is the same as Fig. D.1. Both the results from this work (red) and Ref. 42 are shown.

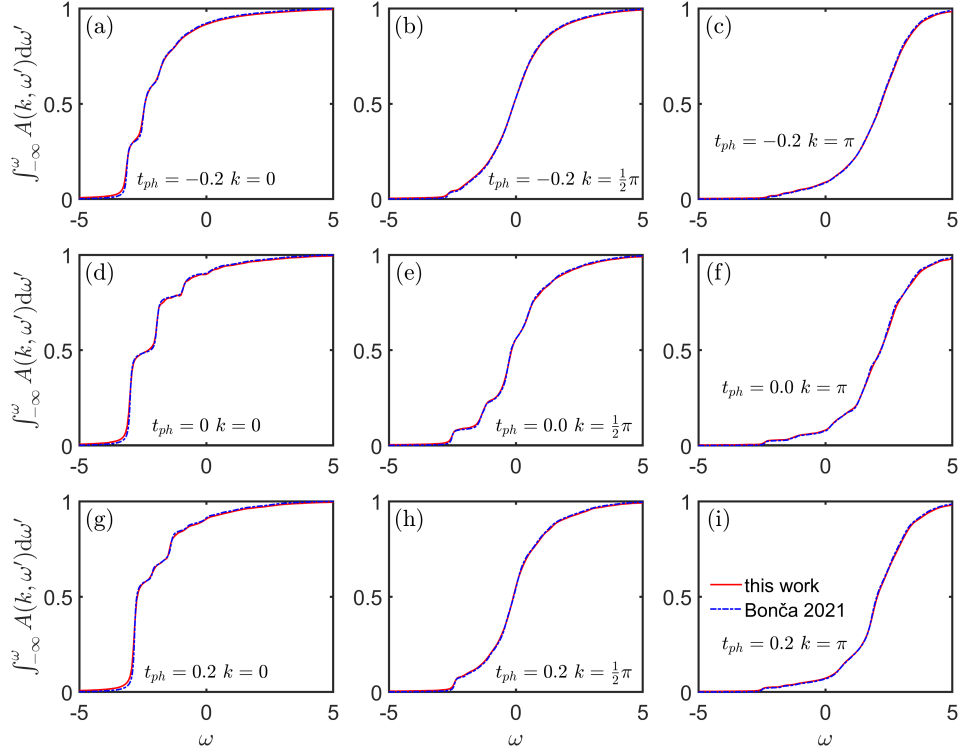


FIG. D.3. Same as Fig. D.2 but for the partially integrated spectral function.

Appendix E: Path integral representation of electron density

We consider a nonequilibrium diffusion problem. We place an electron at the origin of an initially empty lattice, $|\psi\rangle = c_0^\dagger|0\rangle$. We monitor the ensuing evolution of the electron density:

$$\rho(x, t) = \langle 0 | c_0 e^{iHt} c_x^\dagger c_x e^{-iHt} c_0^\dagger | 0 \rangle, \quad (\text{E.1})$$

where H is the Hamiltonian Eq. (A.1). In this section, we derive a path integral representation for $\rho(x, t)$.

First, we trotterize the time evolution and insert the resolution of identity by electron position eigenstates:

$$\begin{aligned} \rho(x, t) = & \sum_{\{x^-\}} \sum_{\{x^+\}} \langle x_0^- | e^{i\epsilon K} | x_1^- \rangle \langle x_1^- | e^{i\epsilon K} | x_2^- \rangle \cdots \langle x_{M-1}^- | e^{i\epsilon K} | x_M^- \rangle \langle x_M^- | e^{-i\epsilon K} | x_{M-1}^+ \rangle \cdots \langle x_2^+ | e^{-i\epsilon K} | x_1^+ \rangle \langle x_1^+ | e^{-i\epsilon K} | x_0^+ \rangle \\ & \times \langle \phi | e^{i\frac{\epsilon}{2}V(x_0^-)} e^{i\epsilon V(x_1^-)} \cdots e^{i\epsilon V(x_{M-1}^-)} e^{i\frac{\epsilon}{2}V(x_M^-)} e^{-i\frac{\epsilon}{2}V(x_M^+)} e^{-i\epsilon V(x_{M-1}^+)} \cdots e^{-i\epsilon V(x_1^+)} e^{-i\frac{\epsilon}{2}V(x_0^+)} | \phi \rangle. \end{aligned} \quad (\text{E.2})$$

Here, $\{x^+\}$ and $\{x^-\}$ label the electron position on the forward and backward branch of the Keldysh contour. We impose the boundary condition $x_0^\pm = 0$ and $x_M^\pm = x$. $V(x)$ is the same as Eq. (A.5).

Second, we perform a change of variables from the electron position to the displacements, $s_j^\pm = x_j^\pm - x_{j-1}^\pm$. Using these, we find:

$$\rho(x, t) = \sum_{\{s^-\}} \sum_{\{s^+\}} \Delta_x(\{s^-\}) \Delta_x(\{s^+\}) A_0^*(\{s^-\}) A_0(\{s^+\}) I(\{s^-\}, \{s^+\}). \quad (\text{E.3})$$

The functional Δ_x ensures that the electron reaches x at time t :

$$\Delta_x(\{s^\pm\}) = \delta(x - \sum_{j=1}^M s_j^\pm). \quad (\text{E.4})$$

A_0 is the amplitude of a free particle defined in Sec. B. The amplitude on the forward and backward branches are complex conjugates. I is the phonon influence functional:

$$\begin{aligned} I(\{s^-\}, \{s^+\}) &= \langle \phi | U^\dagger(s_1^-) U^\dagger(s_2^-) \cdots U^\dagger(s_M^-) U(s_M^+) \cdots U(s_2^+) U(s_1^+) | \phi \rangle \\ &= \langle \phi | U^{-1}(s_1^-) U^{-1}(s_2^-) \cdots U^{-1}(s_M^-) U(s_M^+) \cdots U(s_2^+) U(s_1^+) | \phi \rangle. \end{aligned} \quad (\text{E.5})$$

Here, we have used the same trick as the main text, namely using the translation operator to make the dependence on s explicit. $U(s) = e^{-i\frac{\epsilon}{2}V(0)}T(-s)e^{-i\frac{\epsilon}{2}V(0)}$ is the same as before. The second line follows from the unitarity of $U(s)$.

Third, we exponentiate the influence functional. For the time evolution on the forward branch, we use the recursion relation from Sec. B:

$$\begin{pmatrix} S_j \\ z_j \\ 1 \end{pmatrix} = B(s_j^+) \begin{pmatrix} S_{j-1} \\ z_{j-1} \\ 1 \end{pmatrix}. \quad (\text{E.6a})$$

For the time evolution on the backward branch, we exploit the fact that $U^{-1}(s^-)$ is the inverse of $U(s)$:

$$\begin{pmatrix} S_j \\ z_j \\ 1 \end{pmatrix} = B^{-1}(s_j^-) \begin{pmatrix} S_{j-1} \\ z_{j-1} \\ 1 \end{pmatrix}. \quad (\text{E.6b})$$

The exponentiated form of the influence functional thus reads:

$$I(\{s^-\}, \{s^+\}) = e^{\lambda^2 S(\{s^-\}, \{s^+\})}, \quad (\text{E.7})$$

with

$$S(\{s^-\}, \{s^+\}) = \psi_L B^{-1}(s_1^-) B^{-1}(s_2^-) \cdots B^{-1}(s_M^-) B(s_M^+) \cdots B(s_2^+) B(s_1^+) \psi_R. \quad (\text{E.8})$$

The boundary vectors $\psi_L = (1, 0, 0)$ and $\psi_R = (0, 0, 1)^T$.

We therefore obtain the flow equation for the quantum amplitude $A(\{s^-\}, \{s^+\}) \equiv I(\{s^-\}, \{s^+\}) A_0(\{s^-\}, \{s^+\})$:

$$\frac{dA(\{s^-\}, \{s^+\})}{d\lambda^2} = S(\{s^-\}, \{s^+\}) A(\{s^-\}, \{s^+\}). \quad (\text{E.9})$$

The initial condition is:

$$A(\{s^-\}, \{s^+\}) = A_0^*(\{s^-\}) A_0(\{s^+\}). \quad (\text{E.10})$$

Solving the flow equation effects the compression of A .

In the final step, we need to contract A with Δ . It is then necessary to recast Δ in MPS form. Here, we use the translation matrix $T(x)$:

$$T(x)|y\rangle = |x+y\rangle, \quad (\text{E.11})$$

where $|x\rangle$ is the electro position eigenstate. It is then easy to see:

$$\Delta_x(\{s^+\}) = \langle x | T(s_M^+) \cdots T(s_2^+) T(s_1^+) | 0 \rangle. \quad (\text{E.12})$$

The above is an MPS with bond dimension N . The MPS expression for $\Delta_x(\{s^-\})$ can be found in the same vein.